PHYSICAL REVIEW C **88**, 044335 (2013)

Collective and noncollective excitations in ^{122}Te

Somnath Nag and A. K. Singh
Department of Physics & Meteorology, Indian Institute of Technology Kharagpur, Kharagpur, IN 721302, India

I. Ragnarsson
Division of Mathematical Physics, LTH, Lund University, Box 118, S-221 Lund, Sweden

H. Hübel, A. Al-Khatib, P. Bringel, C. Engelhardt, and A. Neußer-Neffgen
Helmholtz-Institut für Strahlen- und Kernphysik, Universität Bonn, Nussallee 14-16, D-53115 Bonn, Germany

G. B. Hagemann, B. Herskind, and G. Sletten
Niels Bohr Institute, Blegdamsvej 17, DK-2100 Copenhagen Ø, Denmark

M. P. Carpenter, R. V. F. Janssens, T. L. Khoo, and T. Lauritsen
Physics Division, Argonne National Laboratory, Argonne, Illinois 60439, USA

R. M. Clark and P. Fallon
Nuclear Science Division, Lawrence Berkeley National Laboratory, Berkeley, California 94720, USA

G. Benzoni
INFN, Sezione di Milano, I-20133 Milano, Italy

A. Bracco and F. Camera
Dipartimento di Fisica, Universita di Milano and INFN, Sezione di Milano, I-20133 Milano, Italy

P. Chowdhury
Department of Physics, University of Massachusetts Lowell, Lowell, Massachusetts 01854, USA
(Received 5 August 2013; revised manuscript received 18 September 2013; published 31 October 2013)

High-spin states in ^{122}Te were populated in the reaction ^{82}Se(^{48}Ca, $\alpha 4n$)^{122}Te at a beam energy of 200 MeV and γ-ray coincidences were measured with the Gammasphere spectrometer. The previously known level scheme was extended to considerably higher spin. Maximally aligned states and several high-energy transitions feeding into some of these levels were observed. In addition, seven collective high-spin bands were discovered for the first time in this nucleus. The experimental results are compared with cranked Nilsson-Strutinsky model calculations and possible configuration assignments to the new high-spin structures are discussed.

DOI: 10.1103/PhysRevC.88.044335 PACS number(s): 23.20.Lv, 23.20.En, 27.60.+j, 21.60.Ev

I. INTRODUCTION

The mass region around $A = 120$ is known for shape coexistence and the associated interplay between collective and noncollective degrees of freedom. Deformation changes are induced by the alignment of high-j nucleons, in particular protons and neutrons in $h_{11/2}$ orbitals, which have opposite shape-driving effects [1]. The proton Fermi surface lies in the lower part of the $h_{11/2}$ subshell and the neutron Fermi surface is located in the middle to upper region of that shell. Thus, alignments of protons in low-Ω, $h_{11/2}$ orbitals induce prolate shapes, while the aligned neutrons in high-Ω, $h_{11/2}$ orbitals drive towards oblate shapes. The coexistence of prolate and oblate shapes leads to a competition between collective and noncollective excitations [2,3]. These phenomena have been studied in a variety of nuclei; e.g., in neutron deficient Sn [4], Sb [5–7], and Te isotopes [8–10].

For the nuclei in this mass region with a small number of particles outside the ^{114}Sn core, the total angular momentum obtained by coupling the individual spins of all valence particles is limited. Recently, maximally aligned states with 8 to 11 particles were observed [10–13]. Moreover, states with one or two particles antialigned with respect to the rotation axis of the other valence particles were discovered in ^{120}Te [10] and ^{123,125}I [11,12]. In ^{121}I [13], ^{123}I [12], ^{123}Cs [14], and ^{124}Ba [15], low-intensity, high-energy γ-ray transitions were found to feed the maximally aligned states. These transitions result from core-breaking excitations.

In several recent studies, high-spin rotational bands with large deformation were observed in nuclei with neutron number $N = 68$–72; i.e., in ^{120}Te [10], ^{123}I [12], ^{125}I [16], ^{125}Xe, [17], ^{126}Xe [18], and ^{124}Ba [15]. Some of these sequences extend into the spin-60 region. For ^{125}Xe [17] and ^{126}Xe [18], quadrupole deformation parameters of $\varepsilon_2 = 0.25$–0.35 were deduced from Doppler-shift attenuation measurements (DSAM).

In this paper, the results of a spectroscopic investigation of the high-spin structure of ^{122}Te are presented. The previously

known level scheme [19–22] is extended to considerably higher spin. Maximally aligned states and high-energy transitions originating from core-breaking excitations have been observed. Moreover, seven rotational bands with characteristics similar to the high-spin bands in neighboring nuclei have been discovered. Possible configurations for the observed structures are discussed within the framework of the cranked Nilsson-Strutinsky (CNS) model.

In Sec. II, details of the experimental procedure and the data analysis are given. The experimental results and the level scheme are presented in Sec. III. Possible configuration assignments to the new structures are discussed in Sec. IV, which is followed by a brief summary in Sec. V.

II. EXPERIMENTAL DETAILS AND ANALYSIS

Excited states in ^{122}Te were populated in the reaction ^{82}Se(^{48}Ca,$\alpha 4n$)^{122}Te with a nominal beam energy of 205 MeV. The ^{48}Ca beam, with an average current of 1.5 nA, was provided by the ATLAS accelerator at Argonne National Laboratory. The target consisted of a 0.5 mg/cm^2 thick, 99.8% enriched, ^{82}Se foil, evaporated on a 0.5 mg/cm^2 Au backing. A protective Au layer of 0.08 mg/cm^2 covered the ^{82}Se foil. The backing faced the beam and reduced the beam energy to 200 MeV at mid target. The target was mounted on four quadrants of a rotating wheel and the beam was slightly defocused and wobbled horizontally by a few millimeters to prevent heating and evaporation of the Se layer.

Gamma-ray coincidence events were detected using the Gammasphere spectrometer [23] consisting of 100 Compton-suppressed Ge detectors in this experiment. A total of 2.8×10^9 events with Ge fold $\geqslant$5 were recorded in seven days of beam time and stored on magnetic tape. In the reaction, the dominant channels were $4n$, $5n$, $6n$, $p4n$, and $\alpha 4n$, populating ^{126}Xe, ^{125}Xe, ^{124}Xe, ^{125}I, and ^{122}Te, respectively.

In the off-line analysis, the calibrated and gain-matched coincidence events were sorted into γ-γ matrices, γ-γ-γ cubes, and γ-γ-γ-γ hypercubes using the RADWARE software package [24].

Two matrices were sorted for the angular distribution analysis. The first one included the events detected in detectors at forward and backward directions (fb), with average angles of $\approx$35° and $\approx$145°, respectively, on one axis and those detected in all detectors on the other axis (all). The second matrix consisted of counts registered in detectors near 90° on one axis (90) and those in all detectors again on the second axis. Angular distribution ratios, R_θ, were determined by setting gates on these matrices with events detected in all detectors. The intensity ratio

$$R_\theta = \frac{I\left(\gamma_1^{fb}, \gamma_2^{all}\right)}{I\left(\gamma_1^{90}, \gamma_2^{all}\right)}$$

distinguishes between stretched dipole and stretched quadrupole transitions with values of about 0.75 and 1.4, respectively. As usual, stretched quadrupole transitions were assumed to be of $E2$ multipolarity.

III. RESULTS AND LEVEL SCHEME

The level scheme of ^{122}Te, based on both present and previous results [19,20], is displayed in Fig. 1. The positive-parity ground band was established up to $I^\pi = 10^+$ and 12^+ in investigations by Chowdhury *et al.* [21] and Lee *et al.* [22], respectively, and was later extended up to $I^\pi = 16^+$ by Paul *et al.* [19]. Nag *et al.* [20] reported positive-parity levels up to $I = (25)$ and several side branches.

In the present investigation, the previously observed transitions and the spin and parity assignments of the low-spin part of the level scheme are confirmed. The level scheme is extended up to states with spins close to $I = 50$. The highest-spin states are reached in the seven new rotational bands, labeled $b1$ to $b7$ in Fig. 1. Gamma-ray energies, relative intensities, angular distribution ratios, deduced multipolarities, and spin assignments are summarized in Table I.

In the following, only the placements of the more strongly populated new levels in the medium- and high-spin part of the scheme of Fig. 1 will be explained.

A. Medium-spin states

Three examples of triple-gated γ-ray coincidence spectra with transitions from the low- and medium-spin regions are presented in Fig. 2. The spectrum in the upper panel (a) was created with gates on transitions of the ground band, labeled a in Fig. 1. It highlights its extension by a cascade of $E2$ transitions up to the $I^\pi = 22^+$ level at 8268 keV as well as the presence of the side band labeled b. The positive-parity band continues further up in the irregular sequence labeled e. The center (b) and lower (c) panels highlight transitions of the negative-parity sequences c and d, respectively.

The $I^\pi = 22^+$ state decays into the ground band and via a rather strong cascade b of transitions with energies of 1185, 417, 558, 394, 424, and 609 keV into the $I^\pi = 14^+$ level at 4681 keV. This sequence was reported already by Nag *et al.* [20]. The intensity ratios, R_θ, for the 1185-, 417-, 394-, and 609-keV lines are compatible with a stretched dipole nature, whereas stretched $E2$ multipolarity is assigned to the 558- and 424-keV γ rays; see Table I. The ordering of the transitions within cascade b is based on their intensities and is further supported by the presence of several decay-out branches. Prominent cascades are the sequence with energies of 961, 874, and 719 keV, linking the $19^{(-)}$ state of branch b to the 14^+ level of ground band a, and that with energies of 194, 613, and 627 keV, which establishes a decay path from the $18^{(-)}$ state of branch b to the 16^+ level of band a; see Fig. 1. Furthermore, sequence b decays into branches c and d through the 661- and 232-keV transitions, respectively, feeding the (16^-) and (17^-) states. A cascade with an $E2$ γ ray of 540 keV and three dipole transitions of 700, 605, and 521 keV was placed on top of sequence d.

The stretched dipole transitions with energies of 669 and 324 keV feed into the ground band at the $I^\pi = 16^+$ level. The intensity of the 626-keV line could not be determined due to the presence of other close-lying transitions. The 7026-keV state of this sequence is connected by the 745-keV γ ray with the $I^\pi = 20^+$, 7771-keV level of the ground band.

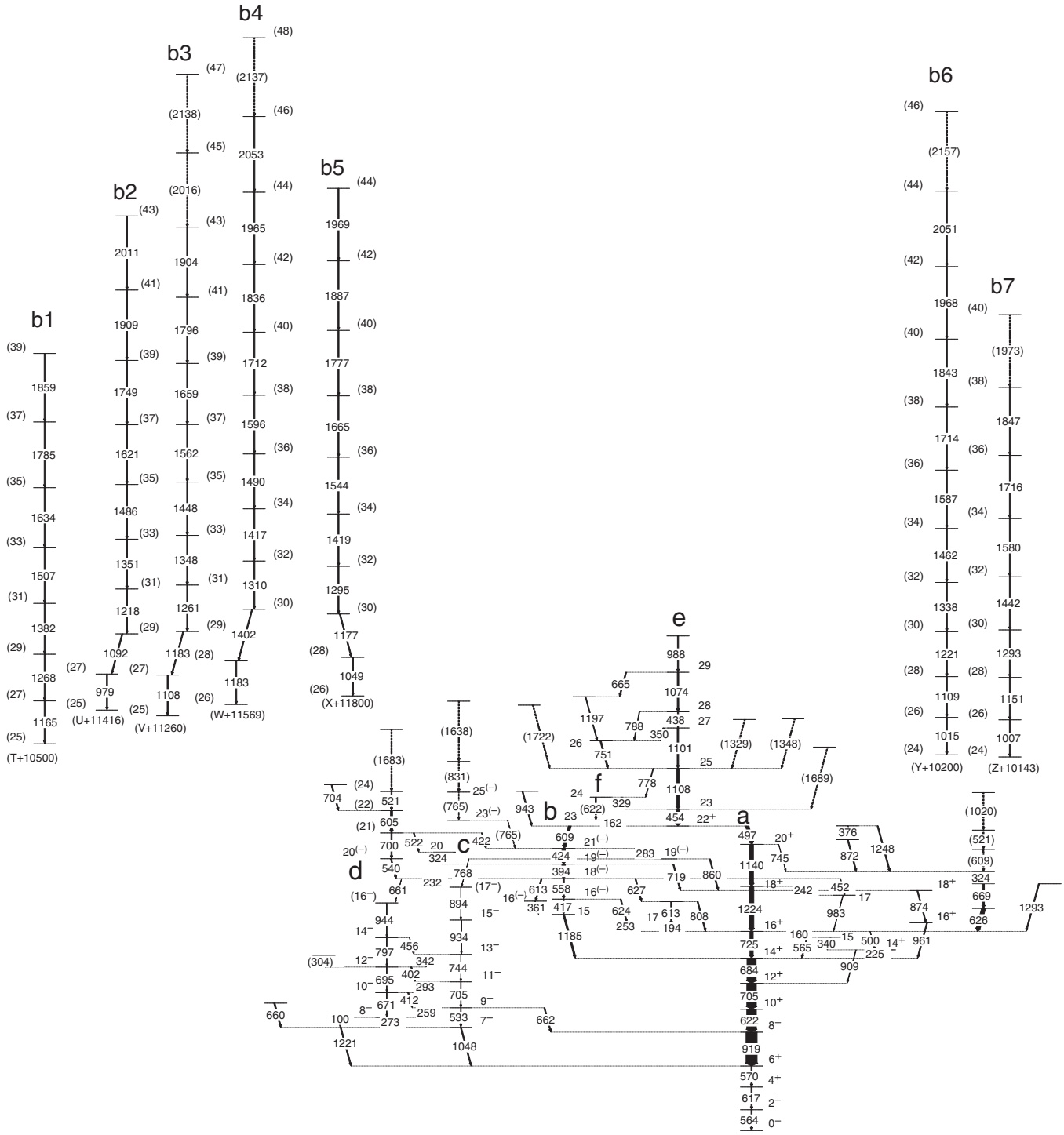

FIG. 1. Level scheme of ^{122}Te.

Above the $I^{\pi} = 22^{+}$ state, the lines with energies of 454, 1108, 1101, 438, 1074, and 988 keV form the continuation e of the positive-parity yrast levels. A stretched dipole character is obtained for the 454-, 438-, and 1074-keV transitions, whereas the 1108- and 1101-keV γ rays exhibit a stretched $E2$ character. The angular distribution ratio for the 988-keV line could not be determined. The 665-, 1197-, and 751-keV transitions connect the $I = 29$ level at 12 443 keV with the $I = 25$ state at 9830 keV.

Three low-intensity γ rays with energies of 1329, 1348, and 1722 keV feed into the level with spin $I = 25$ of sequence e; another one, with an energy of 1689 keV, populates the $I = 23$ state. Some of these lines lie close to in-band transitions of the high-spin bands, see below, and have to be regarded as tentative.

TABLE I. Gamma-ray energies, intensities, angular distribution ratios, spin assignments, level energies, and γ-ray multipolarities for transitions in ^{122}Te.

Energy E_γ[a] (keV)	Intensity I_γ	Intensity ratio R_θ	$I_i^\pi \rightarrow I_f^\pi$	Level energy E_i (keV)	Assigned multipolarity
100.5			$\rightarrow$	3072.5	
160.2	35(10)	0.79(4)	$16^+ \rightarrow 15$	5406.3	$M1$ or $E1$
161.8	15(6)	0.69(8)	$23 \rightarrow 22^+$	8429.9	$M1$ or $E1$
194.2	17(6)	0.71(8)	$17 \rightarrow 16^+$	5600.5	$M1$ or $E1$
224.9	4(1)		$14^+ \rightarrow 14^+$	4905.8	
232.5		0.49(19)	$18^{(-)} \rightarrow (17^-)$	6840.8	$(M1)$
241.6			$18^+ \rightarrow 17$	6630.6	$M1$ or $E1$
253.2			$\rightarrow 16^+$	5659.5	
259.5			$9^- \rightarrow 8^-$	3332.0	
273.4	5(2)		$8^- \rightarrow 7^-$	3072.5	$M1$
282.9	18(7)	1.20(20)	$21^{(-)} \rightarrow 19^{(-)}$	7658.7	$(E2)$
293.0			$11^- \rightarrow 10^-$	4036.8	$M1$
(304.4)			$\rightarrow 12^-$	4743.5	
324.2[b]	23(5)	0.61(4)	$\rightarrow$	7025.7	$M1$ or $E1$
324.2[b]	8(3)	0.61(4)	$20 \rightarrow 19^{(-)}$	7558.6	$M1$ or $E1$
329.4	10(4)	0.75(20)	$24 \rightarrow 23$	9051.7	$M1$ or $E1$
340.3	18(6)	0.64(20)	$15 \rightarrow 14^+$	5246.1	$M1$ or $E1$
341.5	4(2)		$13^- \rightarrow 12^-$	4780.6	$M1$ or $E1$
349.9	11(4)	0.43(20)	$27 \rightarrow 26$	10930.5	$M1$ or $E1$
361.2	13(4)	0.63(4)	$16^{(-)} \rightarrow 15$	6227.5	$M1$ or $E1$
376.4	2(1)		$\rightarrow$	8273.6	
393.6	79(14)	0.91(7)	$19^{(-)} \rightarrow 18^{(-)}$	7234.4	$(M1)$
402.3			$12^- \rightarrow 11^-$	4439.1	$M1$
411.8			$10^- \rightarrow 9^-$	3743.8	$M1$
416.8	21(7)	0.87(6)	$16^{(-)} \rightarrow 15$	6283.1	$M1$ or $E1$
421.6			$(21) \rightarrow 21^{(-)}$	8080.3	$M1$ or $E1$
424.3	75(11)	1.38(30)	$21^{(-)} \rightarrow 19^{(-)}$	7658.7	$(E2)$
438.0	24(8)	0.54(21)	$28 \rightarrow 27$	11368.5	$M1$ or $E1$
451.8			$18^{(-)} \rightarrow 17$	6840.8	$M1$ or $E1$
454.2	82(12)	0.77(4)	$23 \rightarrow 22^+$	8722.3	$M1$ or $E1$
455.8			$14^- \rightarrow 13^-$	5236.4	$M1$
497.5	77(12)	1.46(20)	$22^+ \rightarrow 20^+$	8268.1	$E2$
500.5			$16^+ \rightarrow 14^+$	5406.3	$E2$
520.6	23(5)	1.24(30)	$(24) \rightarrow (22)$	9205.8	$(E2)$
(521.3)			$\rightarrow$	8155.8	
521.7	23(5)	0.66(32)	$(21) \rightarrow 20$	8080.3	$(M1$ or $E1)$
532.9	14(4)	1.30(9)	$9^- \rightarrow 7^-$	3332.0	$E2$
539.5	24(6)	1.67(9)	$20^{(-)} \rightarrow 18^{(-)}$	7380.3	$(E2)$
557.7	31(9)	1.32(18)	$18^{(-)} \rightarrow 16^{(-)}$	6840.8	$(E2)$
564.0			$2^+ \rightarrow 0^+$	564.0	$E2$
565.2			$15 \rightarrow 14^+$	5246.1	$M1$ or $E1$
570.0		1.26(10)	$6^+ \rightarrow 4^+$	1751.0	$E2$
604.9	46(11)	1.00(20)	$(22) \rightarrow (21)$	8685.2	$(M1$ or $E1)$
(608.8)			$\rightarrow$	7634.5	
609.4	64(13)	0.73(16)	$22^+ \rightarrow 21^{(-)}$	8268.1	$(E1)$
613.3			$18^{(-)} \rightarrow 16^{(-)}$	6840.3	$(E2)$
613.4			$\rightarrow 17$	6213.9	
617.0		1.16(10)	$4^+ \rightarrow 2^+$	1181.0	$E2$
621.6	216(11)	1.60(14)	$10^+ \rightarrow 8^+$	3291.2	$E2$
(621.8)			$24 \rightarrow 23$	9051.7	$M1$ or $E1$
623.6[c]			$16^{(-)} \rightarrow$	6283.1	
626.3[c]	80(18)		$\rightarrow 16^+$	6032.6	
626.9[c]			$18^{(-)} \rightarrow$	6840.8	
660.0			$\rightarrow 7^-$	3459.1	
660.6	3(1)	1.38(55)	$18^{(-)} \rightarrow (16^-)$	6840.8	$(E2)$

TABLE I. (*Continued*.)

Energy E_γ[a] (keV)	Intensity I_γ	Intensity ratio R_θ	$I_i^\pi \rightarrow I_f^\pi$	Level energy E_i (keV)	Assigned multipolarity
662.4			$9^- \rightarrow 8^+$	3332.0	$E1$
664.6			$29 \rightarrow$	12442.6	
668.9	42(10)	0.93(16)	$\rightarrow$	6701.5	$M1$ or $E1$
671.3	5(2)		$10^- \rightarrow 8^-$	3743.8	$E2$
684.5	206(16)	1.39(30)	$14^+ \rightarrow 12^+$	4680.9	$E2$
695.3	4(1)		$12^- \rightarrow 10^-$	4439.1	$E2$
700.0		0.76(10)	$(21) \rightarrow 20^{(-)}$	8080.3	($M1$ or $E1$)
704.0			$\rightarrow (22)$	9389.2	
704.8	12(4)		$11^- \rightarrow 9^-$	4036.8	$E2$
705.2	215(16)	1.49(10)	$12^+ \rightarrow 10^+$	3996.4	$E2$
718.9			$19^{(-)} \rightarrow 18^+$	7234.4	($E1$)
725.4	74(4)	1.36(11)	$16^+ \rightarrow 14^+$	5406.3	$E2$
743.8	5(2)		$13^- \rightarrow 11^-$	4780.6	$E2$
744.9	2(1)		$20^+ \rightarrow$	7770.6	$M1$ or $E1$
750.8	31(9)	0.78(2)	$26 \rightarrow 25$	10580.6	$M1$ or $E1$
(765.2)[d]	28(5)	1.50(30)	$23^{(-)} \rightarrow 21^{(-)}$	8423.9	($E2$)
(765.2)[d]		1.50(30)	$25^{(-)} \rightarrow 23^{(-)}$	9189.1	($E2$)
767.5	4(2)		$19^{(-)} \rightarrow (17^-)$	7375.8	($E2$)
778.1	15(5)	0.77(20)	$25 \rightarrow 24$	9829.8	$M1$ or $E1$
787.9	15(5)		$28 \rightarrow 26$	11368.5	$E2$
797.3	2(1)		$14^- \rightarrow 12^-$	5236.4	$E2$
807.6			$\rightarrow 16^+$	6213.9	
(830.8)			$\rightarrow 25^{(-)}$	10019.9	
860.4			$19^{(-)} \rightarrow 18^+$	7375.8	($E1$)
871.5	3(1)		$\rightarrow$	7897.5	
873.8	22(11)	1.55(25)	$18^+ \rightarrow 16^+$	6515.5	$E2$
893.7	3(1)		$(17^-) \rightarrow 15^-$	6608.3	($E2$)
909.4	11(8)	1.50(22)	$14^+ \rightarrow 12^+$	4905.8	$E2$
918.6	250(17)	1.33(9)	$8^+ \rightarrow 6^+$	2669.6	$E2$
934.0	3(1)		$15^- \rightarrow 13^-$	5714.6	$E2$
943.4			$\rightarrow 22^+$	9211.5	
943.8	3(1)		$(16^-) \rightarrow 14^-$	6180.2	($E2$)
960.7	25(10)	1.15(14)	$16^+ \rightarrow 14^+$	5641.6	$E2$
982.7	7(3)	0.48(8)	$17 \rightarrow 16^+$	6389.0	$M1$ or $E1$
987.5			$\rightarrow 29$	13430.1	
(1020.0)			$\rightarrow$	9175.8	
1048.1	26(8)		$7^- \rightarrow 6^+$	2799.1	$E1$
1074.1	34(3)	0.32(25)	$29 \rightarrow 28$	12442.6	$M1$ or $E1$
1100.7	33(10)	1.32(27)	$27 \rightarrow 25$	10930.5	$E2$
1107.5	65(6)	1.38(23)	$25 \rightarrow 23$	9829.8	$E2$
1140.0	84(9)	1.35(10)	$20^+ \rightarrow 18^+$	7770.6	$E2$
1185.4	37(4)	0.80(10)	$15 \rightarrow 14^+$	5866.3	$M1$ or $E1$
1197.4	18(3)		$\rightarrow 26$	11778.0	
1221.0			$\rightarrow 6^+$	2972.0	
1224.3	102(12)	1.22(10)	$18^+ \rightarrow 16^+$	6630.6	$E2$
1247.9			$\rightarrow$	8273.6	
1293.2			$\rightarrow 16^+$	6699.5	
(1328.7)			$\rightarrow 25$	11158.5	
(1347.7)			$\rightarrow 25$	11177.5	
(1688.7)			$\rightarrow 23$	10411.0	
(1721.7)			$\rightarrow 25$	11551.5	
Band $b1$					
1165	86(16)		$(27) \rightarrow (25)$	$T+11665$	($E2$)
1268	100		$(29) \rightarrow (27)$	$T+12933$	($E2$)
1382	62(10)		$(31) \rightarrow (29)$	$T+14315$	($E2$)
1507	41(11)		$(33) \rightarrow (31)$	$T+15822$	($E2$)

TABLE I. (*Continued*.)

Energy E_γ [a] (keV)	Intensity I_γ	Intensity ratio R_θ	$I_i^\pi \rightarrow I_f^\pi$	Level energy E_i (keV)	Assigned multipolarity
1634	59(10)		(35) → (33)	$T + 17456$	($E2$)
1785	66(11)		(37) → (35)	$T + 19241$	($E2$)
1859			(39) → (37)	$T + 21100$	($E2$)
Band $b2$					
979[e]	87(13)		(27) → (25)	$U + 12395$	($E2$)
1092[e]	71(12)		(29) → (27)	$U + 13487$	($E2$)
1218	109(15)		(31) → (29)	$U + 14705$	($E2$)
1351	100		(33) → (31)	$U + 16056$	($E2$)
1486	83(13)		(35) → (33)	$U + 17542$	($E2$)
1621	83(13)		(37) → (35)	$U + 19163$	($E2$)
1749	70(12)		(39) → (37)	$U + 20912$	($E2$)
1909	45(9)		(41) → (39)	$U + 22821$	($E2$)
2011			(43) → (41)	$U + 24832$	($E2$)
Band $b3$					
1108[e]			(27) → (25)	$V + 12368$	($E2$)
1183[e]			(29) → (27)	$V + 13551$	($E2$)
1261	100		(31) → (29)	$V + 14812$	($E2$)
1348	83(14)		(33) → (31)	$V + 16160$	($E2$)
1448	72(9)		(35) → (33)	$V + 17608$	($E2$)
1562	65(11)		(37) → (35)	$V + 19170$	($E2$)
1659	37(6)		(39) → (37)	$V + 20829$	($E2$)
1796	44(8)		(41) → (39)	$V + 22625$	($E2$)
1904			(43) → (41)	$V + 24529$	($E2$)
(2016)			(45) → (43)	$V + 26545$	($E2$)
(2138)			(47) → (45)	$V + 28683$	($E2$)
Band $b4$					
1183[e]			(28) → (26)	$W + 12752$	($E2$)
1402[e]	105(24)		(30) → (28)	$W + 14154$	($E2$)
1310	100		(32) → (30)	$W + 15464$	($E2$)
1417	93(40)		(34) → (32)	$W + 16881$	($E2$)
1490	85(15)		(36) → (34)	$W + 18371$	($E2$)
1596	87(15)		(38) → (36)	$W + 19967$	($E2$)
1712	70(10)		(40) → (38)	$W + 21679$	($E2$)
1836	58(12)		(42) → (40)	$W + 23515$	($E2$)
1965	62(11)		(44) → (42)	$W + 25480$	($E2$)
2053			(46) → (44)	$W + 27533$	($E2$)
(2137)			(48) → (46)	$W + 29670$	($E2$)
Band $b5$					
1049[e]	78(11)		(28) → (26)	$X + 12849$	($E2$)
1177[e]	94(15)		(30) → (28)	$X + 14026$	($E2$)
1295	100		(32) → (30)	$X + 15321$	($E2$)
1419	83(15)		(34) → (32)	$X + 16740$	($E2$)
1544	73(12)		(36) → (34)	$X + 18284$	($E2$)
1665	71(12)		(38) → (36)	$X + 19949$	($E2$)
1777	60(11)		(40) → (38)	$X + 21726$	($E2$)
1887	56(10)		(42) → (40)	$X + 23613$	($E2$)
1969	51(10)		(44) → (42)	$X + 25582$	($E2$)
Band $b6$					
1015	100		(26) → (24)	$Y + 11215$	($E2$)
1109			(28) → (26)	$Y + 12324$	($E2$)
1221			(30) → (28)	$Y + 13545$	($E2$)
1338	117(15)		(32) → (30)	$Y + 14883$	($E2$)
1462	156(21)		(34) → (32)	$Y + 16345$	($E2$)

TABLE I. (*Continued*.)

Energy E_γ[a] (keV)	Intensity I_γ	Intensity ratio R_θ	$I_i^\pi \rightarrow I_f^\pi$	Level energy E_i (keV)	Assigned multipolarity
1587	197(30)		(36) → (34)	$Y + 17932$	($E2$)
1714	74(16)		(38) → (36)	$Y + 19646$	($E2$)
1843	86(18)		(40) → (38)	$Y + 21489$	($E2$)
1968	87(18)		(42) → (40)	$Y + 23457$	($E2$)
2051			(44) → (42)	$Y + 25508$	($E2$)
(2157)			(46) → (44)	$Y + 27665$	($E2$)
Band $b7$					
1007	100		(26) → (24)	$Z + 11150$	($E2$)
1151	101(25)		(28) → (26)	$Z + 12301$	($E2$)
1293	81(20)		(30) → (28)	$Z + 13594$	($E2$)
1442	91(27)		(32) → (30)	$Z + 15036$	($E2$)
1580	60(19)		(34) → (32)	$Z + 16616$	($E2$)
1716	69(19)		(36) → (34)	$Z + 18332$	($E2$)
1847			(38) → (36)	$Z + 20179$	($E2$)
(1973)			(40) → (38)	$Z + 22152$	($E2$)

[a]Uncertainties of γ-ray energies lie within 0.2 to 0.6 keV depending on intensity. The uncertainties of γ-ray energies in bands $b1$–$b7$ lie within 2 keV.
[b]Combined angular correlation ratio for both 324.2-keV transitions.
[c]Combined intensity for 623.6-, 626.3-, and 626.9-keV transitions.
[d]Combined intensity and angular correlation measurement for both 765.2-keV γ rays.
[e]Probable decay-out transitions from band.

B. High-spin bands

In Figs. 3 and 4, triple gated γ-ray coincidence spectra of the seven high-spin rotational bands observed in this experiment are displayed. Band 6 is the most intense, gathering about 3.5% of the channel population. The other bands are weaker: their intensities are estimated to lie between 1 and 2%. Due to their low intensity, a determination of angular distribution ratios for the in-band transitions was not possible. It was assumed that

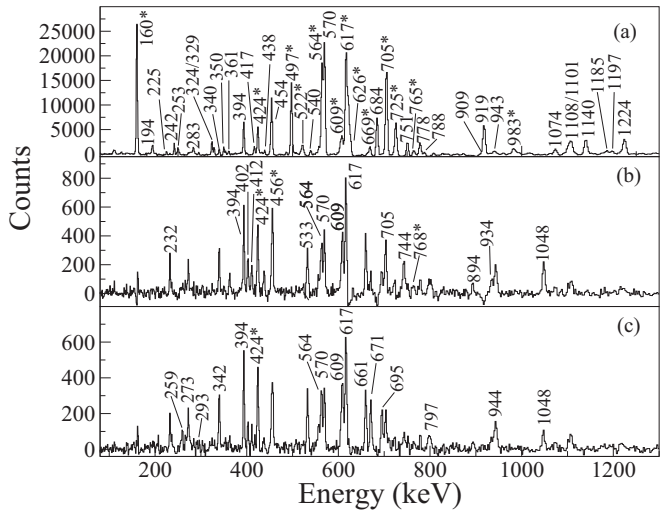

FIG. 2. Sample, summed triple-gated γ-ray coincidence spectra. The spectrum in panel (a) was produced with gates from a list of the 570-, 919-, and 622-keV transitions of the ground band. The spectrum in panel (b) was created with a gate on one γ ray from each of the sets of two transitions with energies of (1048 and 533 keV), (564 and 570 keV), and (394 and 424 keV), respectively. The spectrum in panel (c) was produced with a gate on one transition from each of the sets with (1048 and 273 keV), (564 and 570 keV), and (394 and 424 keV), respectively. Unresolved transitions are marked by asterisks.

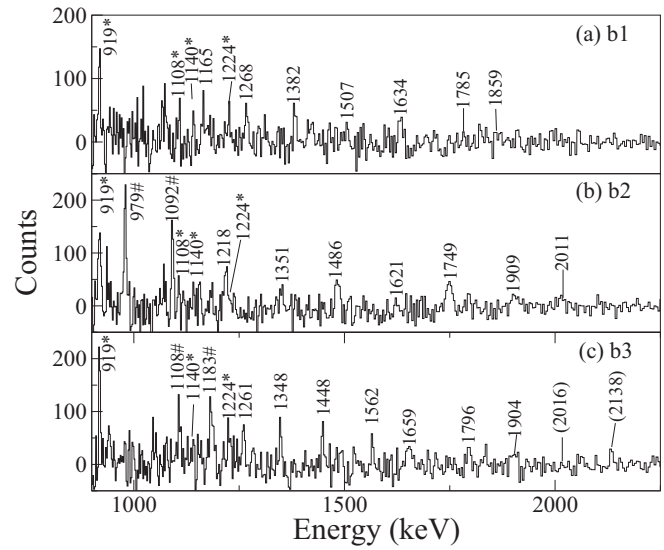

FIG. 3. Summed triple-gated γ-ray coincidence spectra of bands $b1$–$b3$ produced with a single gate from the list of the 564-, 570-, 919-, 622-, 685-, 705-, and 725-keV γ rays and with double gates on all transitions of the respective bands. Lines marked by # signs are possible linking transitions; those marked by * are medium- or low-spin transitions.

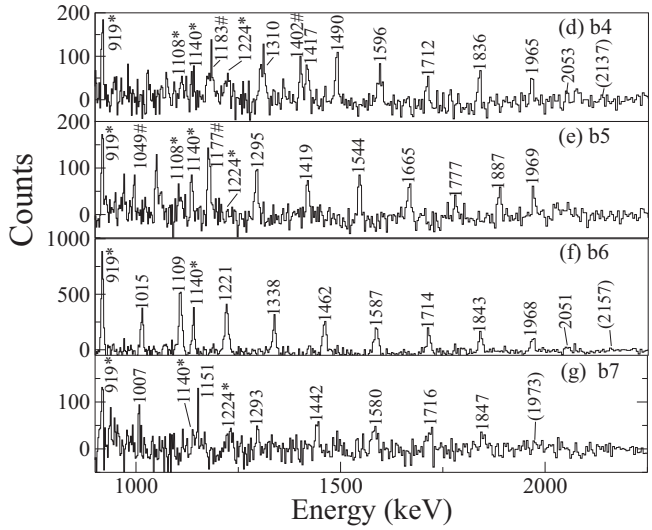

FIG. 4. Summed triple-gated γ-ray coincidence spectra of bands $b4$–$b7$ produced with a single gate from the list of the 564-, 570-, 919-, 622-, 685-, 705-, and 725-keV transitions and with double gates on all γ rays of the respective bands. Lines marked by # signs are possible linking transitions; those marked by * are medium- or low-spin transitions.

they are of $E2$ multipolarity. The ordering of the transitions within the bands is based on their expected rotational behavior as well as their relative intensities in the coincidence spectra. Some γ rays at the bottom are weaker due to (unobserved or unplaced) decay branches to lower-spin levels; see Table I.

All seven bands are in coincidence with ^{122}Te transitions. However, they are not firmly linked to the lower part of the level scheme. The decay paths are probably fragmented, with low-intensity branches to different regions of the level scheme. A major part of the decay appears to proceed via the $I = 23$ and 25 states of sequence e.

First estimates of excitation energies of $b1$–$b7$ were made assuming that weaker bands are located at higher energies and band head spins were chosen to lie about $2\hbar$ above those of levels observed in coincidence. These energy and spin values are similar to those of known connected bands in neighboring nuclei; see below. With these starting values, the behavior of the bands in the excitation energy vs spin plane was compared with results of CNS calculations, see below, which leaded to minor adjustments. Spin values are uncertain by at least $2\hbar$ and excitation energies may vary by about 2 MeV.

IV. DISCUSSION

The structure of the low-spin levels in ^{122}Te was investigated in previous work [19–22]. Here, only the configuration assignments to the new high-spin states will be discussed.

Of special interest are the terminating states, where all spin vectors of the valence particles outside the ^{114}Sn core are aligned. Several high-energy transitions feeding these levels are observed. They are suggested to originate from core-excited states.

The seven unconnected high-spin bands exhibit features similar to those of the long collective bands discovered recently in several nuclei of the region with neutron numbers between $N = 68$ and 72 [10,12,15–18]. Configurations for the new high-spin structures are suggested on the basis of comparisons with the results of CNS calculations.

A. CNS calculations

Within the framework of the CNS approach [25–27], no distinction is made between valence orbitals and the core. The configurations are labeled by the number of particles or holes in orbitals with their main amplitudes in different j shells. Particles in high-j intruder orbitals and in the other j shells can be distinguished [25,28]. Each group of orbitals is further divided according to signature $\alpha = 1/2$ and $\alpha = -1/2$, respectively. The configurations are labeled as $[p_1 p_2, n_1(n_2 n_3)]$, where p_1 is number of proton holes in $g_{9/2}$ levels and p_2 is the number of protons in $h_{11/2}$ orbitals, whereas the number of neutrons occupying $h_{11/2}$, $(h_{9/2} f_{7/2})$, and $i_{13/2}$ orbitals are represented by n_1, n_2, and n_3, respectively.

In the present calculations, the κ and μ parameters derived for the $A = 110$ region have been applied [29]. Total energies are calculated as the sum of the rotating liquid drop energy and the shell energy using the Strutinsky method [30,31]. The Lublin-Strasbourg drop (LSD) [32] with a diffuse surface has been used to estimate the static liquid drop energy. The rigid body moments of inertia are calculated with a radius parameter of $r_0 = 1.16$ fm and a diffuseness of $a = 0.6$ fm [27]. An absolute energy scale based on mass excess has been applied so that different nuclei can be compared. The calculation minimizes the energy for different configurations with respect to the deformation parameters $(\varepsilon_2, \varepsilon_4, \gamma)$ at different spins. Pairing is neglected. Thus, the results of the calculations are applicable in regions where pairing is quenched. However, agreement with experiment is often achieved also in the intermediate-spin region, for $I > 15$ [10,11,33].

B. Medium-spin range

Favored aligned neutron states, involving the particles available outside the ^{114}Sn core, are

$$\nu\left[d_{3/2}^2, h_{11/2}^4\right]; \quad I_{\max}^{\pi} = 16^+, 18^+;$$
$$\nu\left[d_{3/2}^3, h_{11/2}^3\right]; \quad I_{\max}^{\pi} = 15^-;$$
$$\nu\left[d_{3/2}, h_{11/2}^5\right]; \quad I_{\max}^{\pi} = 19^-.$$

The maximum spin values given here can be inferred from the tilted Fermi surface diagram presented in panel (b) of Fig. 5 where the calculated single-particle energies, e_i, are plotted as a function of the spin-projection quantum number, m_i. The orbitals below the straight lines are occupied and the total spin is obtained as the sum of all projections m_i below the lines. Note that the state referred to as $I_{\max}^{\pi} = 16^+$ is formed when four $h_{11/2}$ neutrons couple to spin 16 while the two neutrons in $d_{3/2}$ orbitals are paired to spin 0. They are drawn as filling the $m_i = \pm 1/2$ states in Fig. 5(b).

The favored proton configurations are

$$\pi[(g_{7/2}, d_{5/2})^2]; \quad I_{\max}^{\pi} = 6^+;$$
$$\pi[g_{7/2}, h_{11/2}]; \quad I_{\max}^{\pi} = 9^-.$$

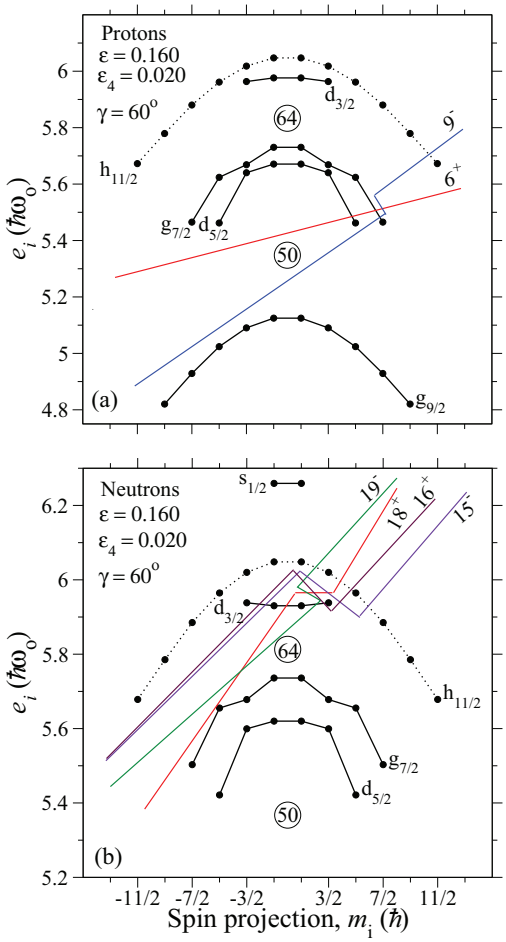

FIG. 5. (Color online) Calculated single-particle energies, e_i, as a function of the spin-projection quantum number, m_i, calculated at $\varepsilon_2 \approx 0.16$, $\gamma = 60°$: (a) for protons and (b) for neutrons. Some low-lying aligned configurations are defined by "straight-line Fermi surfaces," where the orbitals below the lines are occupied and the total spin is obtained as the sum of the projections m_i below the lines.

In this case as well, the maximum spin values are the sums of the projections m_i below the straight lines [panel (a) of Fig. 5]. Coupling these configurations to those for the neutrons provides the I^π quantum numbers for the favored aligned states expected in ^{122}Te.

The experimental excitation energies, relative to a rotating liquid drop energy, for the medium-spin states are plotted in panel (a) of Fig. 6. The calculated energies for the configurations mentioned above are displayed in panel (b) of the figure. Aligned states are highlighted by large open circles and labeled by their spins.

The 16^+ state at 5406 keV may be explained by coupling the protons in $(g_{7/2}, d_{5/2})$ orbitals with $I^\pi_{\max} = 6^+$ to a neutron configuration with $I^\pi_{\max} = 10^+$. This state is formed from two fully aligned $h_{11/2}$ neutrons and is a typical feature of calculations with pairing, but it does not appear in the present, unpaired CNS calculations.

When the neutron configuration with $I^\pi = 16^+$ is coupled to the $(g_{7/2}, d_{5/2})$ proton configuration, it may describe the experimentally observed 22^+ state at 8268 keV. The CNS

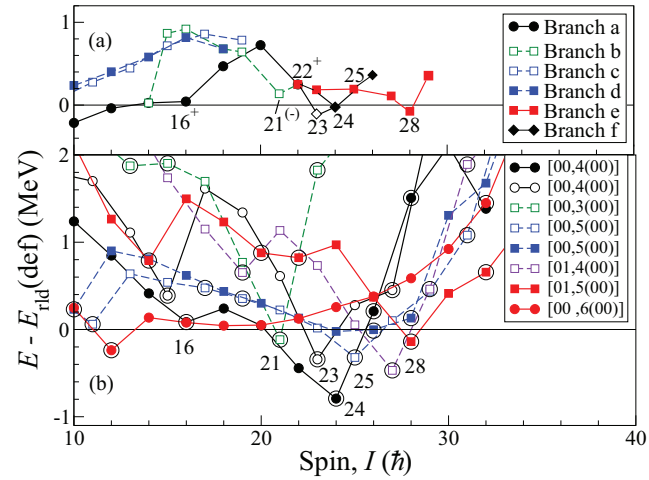

FIG. 6. (Color online) Excitation energies, relative to a rotating liquid drop energy, for observed (a) and calculated (b) valence-space states in ^{122}Te. Calculated states with spin vectors aligned along the oblate symmetry axis are highlighted by large open circles; states corresponding to experimentally observed levels are labeled by their spins.

calculations do not show this state (which has a deformation of $\epsilon_2 \approx 0.16$ and $\gamma \approx 60°$) as a favorable excitation; see Fig. 6(b). However, states with $I^\pi = 22^+$ involving four $h_{11/2}$ neutrons are observed in neighboring ^{120}Te [10] and with $I^\pi = 55/2^-$ in ^{125}I [11]. In these nuclei, the tilted Fermi surfaces give an empty and a filled $d_{3/2}$ shell, respectively, consistent with their lower energy compared with the 22^+ state in ^{122}Te.

The maximum spin that can be generated by the full alignment of the angular momenta of all valence nucleons in the configuration $\pi[g_{7/2}, d_{5/2}]^2_6 \otimes \nu[d^2_{3/2}, (h_{11/2})^4]_{18}$, or [00,4(00)] in the shorthand notation is 24^+. In the calculation of Fig. 6(b), a minimum in energy is found at this spin value. Experimentally, the $I = 23$ levels of sequences e and f at 8429 and 8722 keV, respectively, and the $I = 24$ state at 9051 keV of sequence f lie low in energy. A minimum with $I = 23$ in the CNS calculation corresponds to the maximum-spin state of the [00,4(00)] configuration, where the two $d_{3/2}$ neutrons have signature $\alpha = 1$; i.e., they couple to $I = 1$.

The negative-parity branches c and d are established experimentally up to spins $I = 17$ and 16, respectively. They may correspond to the two signature partners of the configuration $\pi[(g_{7/2}, d_{5/2})^2]_6 \otimes \nu[d_{3/2}, (h_{11/2})^5]_{19}$, or [00,5(00)] in shorthand. The CNS calculations, see Fig. 6(b), show similarities with the observed bands.

In sequence b, a favored level is observed at $I^\pi = 21^-$. A corresponding low-lying state is obtained in the CNS calculation for the configuration [00,3(00)]; see Fig. 6(b). It is built from the 6^+ state of Fig. 5(a), and the 15^- state in panel (b). A similar configuration was found to be favored in the spin range between $I = 19$ and 21 in ^{120}Te [10].

Sequence e exhibits a low-lying level at $I = 28$, as can be seen in the upper panel of Fig. 6. In the calculations, the $I^\pi = 28^+$ state of the configuration $\pi[(g_{7/2}, d_{5/2}), h_{11/2}]_9 \otimes \nu[d_{3/2}, (h_{11/2})^5]_{19}$, or [01,5(00)] in shorthand, is favored. This configuration is proposed for branch e.

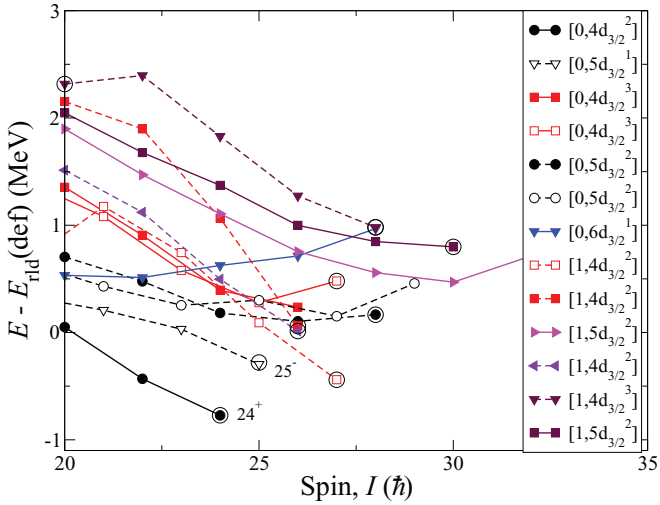

FIG. 7. (Color online) Calculated excitation energies relative to a rotating liquid drop reference for core-breaking configurations. Aligned states are highlighted by open circles and labeled by their spins.

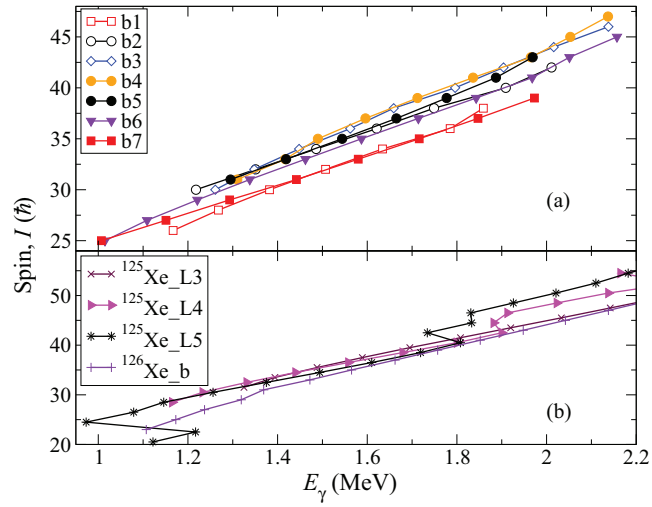

FIG. 8. (Color online) Estimated spins as a function of γ-ray transition energies for the high-spin bands in ^{122}Te, compared with connected bands in neighboring nuclei. The slope of the curves represents the alignment of the bands.

C. Core-excited states

Several high-energy transitions feed levels around $I = 25$; see Fig. 1. Their large energy, between ≈1.2 and 1.7 MeV, indicates that they deexcite core-breaking states. They may involve neutron excitations across the $N = 64$ subshell gap from $(g_{7/2}, d_{5/2})$ into $(d_{3/2}, s_{1/2})$ or $h_{11/2}$ orbitals or proton excitations across the $Z = 50$ shell gap from $(g_{7/2}, d_{5/2})$ into $(d_{3/2}, s_{1/2})$ or $h_{11/2}$ states. However, spin values above $I = 25$ can also be built in configurations with protons excited from $(g_{7/2}, d_{5/2})$ into $h_{11/2}$ orbitals.

In general, low-j orbitals of the $N_{\rm osc} = 64$ shell are not distinguished within the CNS approach. However, for a discussion of core-excited states, a distinction should be made between $(g_{7/2}, d_{5/2})$ and $(d_{3/2}, s_{1/2})$ orbitals. For this purpose, the configurations are labeled as $[p_1, n_1 d_{3/2}^{n_2}]$, where p_1 is the number of protons in $h_{11/2}$ orbitals, and n_1 and n_2 are the numbers of neutrons in $h_{11/2}$ and $(d_{3/2}, s_{1/2})$ states, respectively.

Figure 7 compares calculated excitation energies for the states generated by core excitations of this type. For reference, the valence space configurations terminating at $I = 24^+$ and 25^- with configurations $[0, 4d_{3/2}^2]$ and $[0, 5d_{3/2}^1]$, respectively, are also provided. Neutron excitation across the $N = 64$ gap result in, e.g., the $[0, 5d_{3/2}^2]$, $[0, 6d_{3/2}^1]$, and $[0, 4d_{3/2}^3]$ configurations. In addition, protons occupying $h_{11/2}$ orbitals, coupled to the various neutron excitations, may be considered. A low-lying example is the $[1, 4d_{3/2}^2]$ configuration, also shown in Fig. 6(b), which terminates in an $I = 27^+$ level; see Fig. 7.

D. High-spin bands

The seven new high-spin rotational bands in ^{122}Te exhibit features similar to the long collective bands in neighboring nuclei with neutron numbers N between 68 and 72 [10,12,15–18]. Since these new bands are not linked to the lower-lying states of the level scheme, configuration assignments based on comparisons with CNS calculations can only be viewed as tentative.

In Figs. 8 and 9, the spins as a function of γ-ray energy and the dynamic moments of inertia as a function of rotational frequency, respectively, are compared to selected bands in neighboring nuclei. The similarity of the new bands with, e.g., connected bands in ^{125}Xe [17] and ^{126}Xe [18] is striking. For several bands in these Xe isotopes, deformation parameters ε_2 between 0.25 and 0.35 were deduced from the results of DSAM-type measurements. The deformation of the new bands in ^{122}Te probably lies in this range as well. For comparison, the superdeformed band in ^{132}Ce [34] with $\varepsilon_2 \simeq 0.4$ is included in Fig. 9; its moment of inertia is appreciably larger.

A recent investigation [35] within the framework of the CNS model indicates that the collective bands in this mass

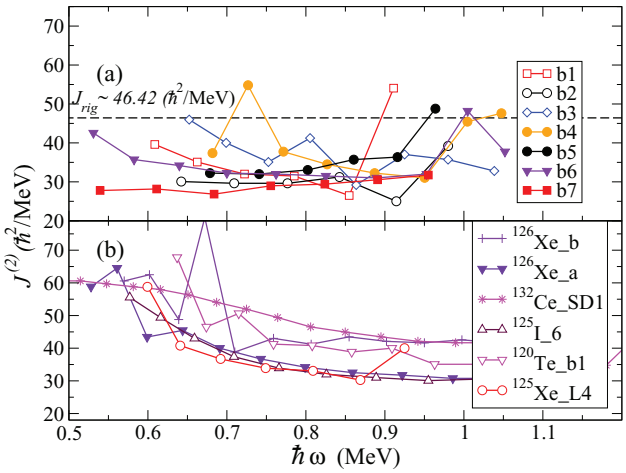

FIG. 9. (Color online) Dynamic moments of inertia, $J^{(2)}$, as a function of rotational frequency. Panel (a) for the high-spin bands in ^{122}Te, panel (b) for similar bands in neighboring nuclei and for a superdeformed band in ^{132}Ce [34].

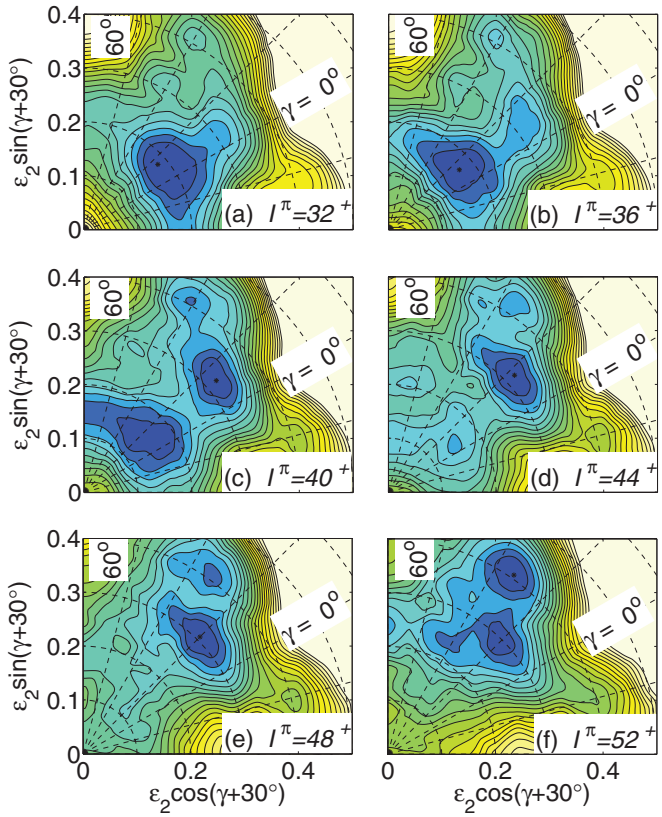

FIG. 10. (Color online) Calculated total energy surfaces for ^{122}Te with the constraint of two $g_{9/2}$ proton holes. The contour line separation is 0.25 MeV.

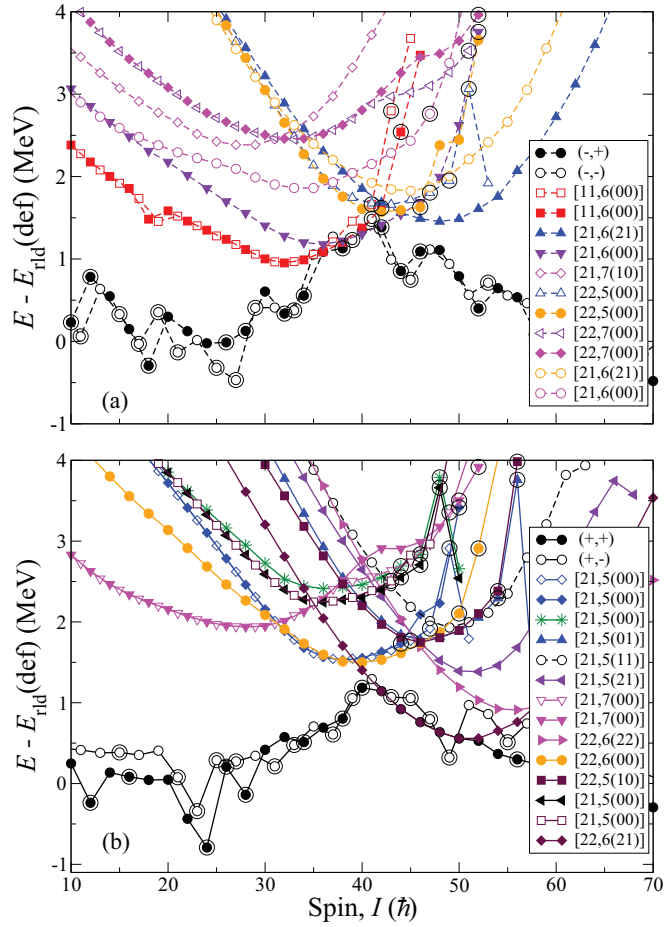

FIG. 11. (Color online) Calculated excitation energies, relative to a rotating liquid drop energy, as a function of spin for low-energy configurations with one or two holes in $g_{9/2}$ orbitals. Panel (a): negative-parity states; panel (b): positive-parity configurations.

region involve proton holes in the $g_{9/2}$ subshell, below the $Z = 50$ gap. In general, it seems that bands with two holes are easier to populate experimentally than those with one hole [29].

Total energy surfaces, computed with the constraint of two $g_{9/2}$ proton holes, are displayed in Fig. 10. At $I^\pi = 32^+$, a prolate minimum is observed with $\varepsilon_2 \approx 0.20$, corresponding to configurations with the neutrons confined to the $N = 50$–82 shell. Around $I^\pi = 40^+$, a second minimum appears at $\varepsilon_2 \approx 0.30$ and $\gamma \approx 15°$, which becomes lowest in energy at higher spins. The most favored configuration in this minimum has three neutrons excited across the $N = 82$ gap; two in $(h_{9/2}, f_{7/2})$ orbitals and one in the $i_{13/2}$ subshell, in addition to the two proton holes in $g_{9/2}$ orbitals. Finally, at $I^\pi = 52^+$, a minimum at $\varepsilon_2 \approx 0.40$, $\gamma \approx 25°$ is lowest in energy, where a second neutron is excited to oscillator-shell $N_{\rm osc} = 6$ orbitals. In addition, protons are excited from the $N_{\rm osc} = 3$ shell.

Low-lying configurations involving one or two $g_{9/2}$ proton holes are presented for various combinations of parity and signature in Fig. 11. Generally, structures involving one $g_{9/2}$ hole either terminate at too low a spin value or lie at higher excitation energy compared to those with two proton holes in the $g_{9/2}$ subshell. The configurations involving two proton holes and neutron excitations across the $N = 64$ gap to $(d_{3/2}, s_{1/2})$ and $h_{11/2}$ orbitals lie low in energy in the spin range of $I = 30$–40. Furthermore, states generated with contributions from $i_{13/2}, h_{9/2}$, and $f_{7/2}$ neutron orbitals become yrast at very high spin. Note, however, that in an extended spin range there is a competition from less-collective states which do not contain $g_{9/2}$ proton holes.

The experimental bands with tentatively chosen excitation energies and spins are displayed in Fig. 12(a) relative to a rotating liquid drop reference. The corresponding energies for calculated configurations, see Fig. 11, which might be assigned to the bands are displayed in Fig. 12(b). The differences between the experimental and calculated energies are presented in panel (c).

If the proton configuration $\pi[(g_{9/2})^{-2}(g_{7/2}, d_{5/2})^3 h_{11/2}]$ with $I_{\rm max} = 22$ is coupled to six $h_{11/2}$ neutrons, it results in the [21,6(00)] structure which is close to the prolate axis at low and intermediate spin values. It is calculated to be lowest in energy among all $\pi(g_{9/2})^{-2}$ configurations in a large spin range. It contains the neutron configuration $(g_{7/2}, d_{5/2})^{-2}(h_{11/2})^6(d_{3/2}, s_{1/2})^2$ and terminates at $I = 48$. Here, two neutrons are excited within the $N_{osc} = 4$ orbitals from $(g_{7/2}, d_{5/2})$ to $(d_{3/2}, s_{1/2})$ levels. This excitation is not seen in the shorthand label because it is not distinguished between these orbitals in the numerical calculations. The [21,6(00)] configuration is a promising candidate for the most intense band *b*6. With the present tentative spin assignment, it is observed one transition short of termination. The difference curve

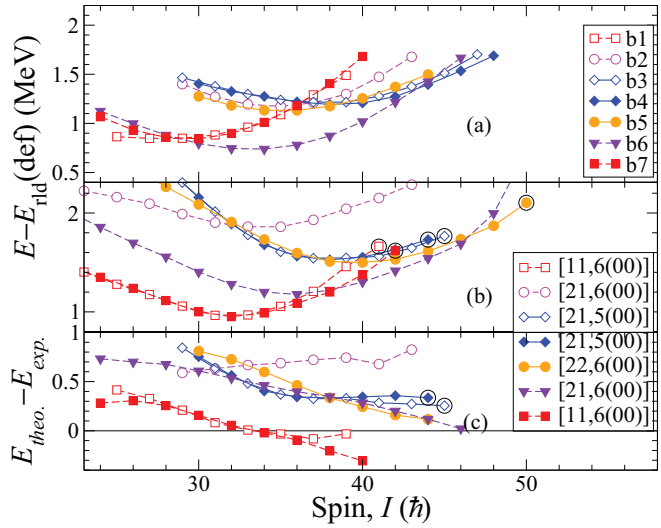

FIG. 12. (Color online) Comparison of observed, panel (a), and calculated, panel (b), excitation energies relative to a rotating liquid drop reference as a function of spin for bands $b1$–$b7$ in ^{122}Te. The difference between the calculated and the experimental excitation energies is shown in panel (c).

between experiment and calculations, displayed in Fig. 12(c), behaves as expected, i.e., the difference increases slowly with decreasing spin indicating the increasing importance of the pairing correlations not included in the CNS calculations.

In the calculations, there is only one configuration with one proton $g_{9/2}$ hole forming a regular band up to $I \sim 40$, where this type of configuration terminate. It is the [11,6(00)] structure which lies low in energy; see Fig. 11(a). The two signature-degenerate branches terminate in the $\pi[(g_{9/2})^{-1}(g_{7/2}, d_{5/2})^3 h_{11/2}] \otimes \nu[(g_{7/2}, d_{5/2})^{-2}(h_{11/2})^6 (d_{3/2}s_{1/2})^2]$ states with $I_{max} = 41$ and 42.

Bands $b1$ and $b7$ are not observed to very high spin. With the presently chosen spin values and excitation energies, they are close to being signature degenerate over their full spin range. When compared with the [11,6(00)] configurations, the difference curves, Fig. 12(c), exhibit a spin dependence similar to that for band $b6$. The absolute values of the two difference curves differ by approximately 0.5 MeV, but they would overlap for a rather small change in the relative excitation energies. The arguments for this interpretation of bands $b1$ and $b7$ would clearly become stronger if they were connected by $M1$ transitions which are expected for bands with one hole in a high-K orbital; see, e.g., Ref. [36].

Bands $b3$, $b4$, and $b5$ have rather similar $E - E_{rld}$ curves. Bands $b3$ and $b4$ are close to being signature degenerate. They are observed well beyond $I = 40$, which implies that they should be assigned to configurations with two proton $g_{9/2}$ holes. It is possible to interpret these as the two signatures of the [21,5(00)] configuration. Band $b5$ may then be assigned to the [22,6(00)] configuration, which has a similar $E - E_{rld}$ curve, as seen in Fig. 12(b). A difficulty with this interpretation is that the I_{max} values for the two [21,5(00)] bands are 44^+, 45^+, whereas the two bands are observed up to $I = 46, 45$ or tentatively even up to $I = 48, 47$. Note, however, that the I_{max} states are formed with two $(g_{7/2}, d_{5/2})$ holes in the $Z = 64$ core and with small changes of the parameters, bands containing more such holes might extend smoothly to higher spins.

Band $b2$ is the weakest band observed and is not observed to very high spin. Therefore, it might be assigned to a configuration with one $g_{9/2}$ hole. However, with the present constraints, no smooth band with features similar to band $b2$ is calculated. In Fig. 12, it has been compared with the unfavored signature of the [21,6(00)] configuration. The favored signature has been assigned to band $b6$; see above. This results in a reasonable difference curve; see Fig. 12(c). However, the spin dependence is different compared with the other bands, underlining the tentative character of this assignment.

V. CONCLUSIONS

High-spin states in ^{122}Te were populated in the ^{82}Se(^{48}Ca,$\alpha 4n$)^{122}Te reaction and γ-ray coincidences were measured with the Gammasphere spectrometer. The level scheme of this nucleus was extended up to $I \simeq 48$. Terminating states within the valence space, high-energy transitions from core-excited states, and seven high-spin rotational bands were observed.

Comparison with CNS calculations allows us to propose configuration assignments to the terminating states. Suggestions are presented for configurations of core-breaking levels and for the high-spin bands. Choosing spins in accordance with those of connected bands in neighboring nuclei and estimating excitation energies from their relative intensities, configurations were assigned for the bands corresponding to the lowest band structures calculated within the framework of the CNS model. Their structures are based on proton excitations from $g_{9/2}$ orbitals coupled to neutron excitations within the $N = 50$–82 valence space.

ACKNOWLEDGMENTS

The authors would like to thank the ATLAS and Gammasphere operations staff for their support. S.N. acknowledges financial support from CSIR, India, under Contract No. 09/081(0704)/2009-EMR-I and help from Dr. P. Singh. This work was supported by the DST, India, under Project No. SR/S2/HEP-09/2005, by the Swedish Science Research Council, by the German BMBF under Contract No. 06 BN 109, by the Danish FNU Council for Natural Sciences, and by the U.S. Department of Energy, Office of Nuclear Physics, under Contracts No. DE-AC02-06CH11357 and No. DE-AC03-76SF00098.

[1] A. Granderath, P. F. Mantica, R. Bengtsson, R. Wyss, P. von Brentano, A. Gelberg, and F. Seiffert, Nucl. Phys. A **597**, 427 (1996).

[2] Y. Liang, R. Ma, E. S. Paul, N. Xu, D. B. Fossan, J.-y. Zhang, and F. Dönau, Phys. Rev. Lett. **64**, 29 (1990).

[3] E. S. Paul, D. B. Fossan, J. M. Sears, and I. Thorslund, Phys. Rev. C **52**, 2984 (1995).
[4] R. Wadsworth *et al*., Phys. Rev. C **50**, 483 (1994).
[5] H. Schnare *et al*., Phys. Rev. C **54**, 1598 (1996).
[6] A. K. Gaigalas, R. E. Shroy, G. Schatz, and D. B. Fossan, Phys. Rev. Lett. **35**, 555 (1975).
[7] R. E. Shroy, A. K. Gaigalas, G. Schatz, and D. B. Fossan, Phys. Rev. C **19**, 1324 (1979).
[8] J. M. Sears *et al*., Phys. Rev. C **55**, 2290 (1997).
[9] S. Juutinen *et al*., Phys. Rev. C **61**, 014312 (1999).
[10] S. Nag *et al*., Phys. Rev. C **85**, 014310 (2012).
[11] P. Singh *et al*., Phys. Rev. C **82**, 034301 (2010).
[12] P. Singh *et al*., Phys. Rev. C **86**, 067305 (2012).
[13] E. S. Paul, J. Simpson, S. Araddad, C. W. Beausang, M. A. Bentley, M. J. Joyce, and J. F. Sharpey-Schafer, J. Phys. G **19**, 913 (1993).
[14] A. K. Singh *et al*., Phys. Rev. C **70**, 034315 (2004).
[15] A. Al-Khatib *et al*., Phys. Rev. C **74**, 014305 (2006).
[16] P. Singh *et al*., Phys. Rev. C **84**, 024316 (2011).
[17] A. Al-Khatib *et al*., Phys. Rev. C **83**, 024306 (2011).
[18] C. Rønn Hansen *et al*., Phys. Rev. C **76**, 034311 (2007).
[19] E. S. Paul, D. B. Fossan, G. J. Lane, J. M. Sears, I. Thorslund, and P. Vaska, Phys. Rev. C **53**, 1562 (1996).
[20] Somnath Nag *et al*. [Eur. Phys. J. A (to be published)].
[21] P. Chowdhury, W. F. Piel, Jr., and D. B. Fossan, Phys. Rev. C **25**, 813 (1982).
[22] C. S. Lee, J. A. Cizewski, D. Barker, R. Tanczyn, G. Kumbartzki, J. Szczepznski, J. W. Gan, H. Dorsett, R. G. Henry, and L. P. Farris, Nucl. Phys. A **528**, 381 (1991).
[23] I. Y. Lee, Nulc. Phys. A **520**, c641 (1990).
[24] D. C. Radford, Nucl. Instrum. Methods Phys. Res. A **361**, 297 (1995).
[25] A. V. Afanasjev and I. Ragnarsson, Nucl. Phys. A **608**, 176 (1996).
[26] T. Bengtsson and I. Ragnarsson, Nucl. Phys. A **436**, 14 (1985).
[27] B. G. Carlsson and I. Ragnarsson, Phys. Rev. C **74**, 011302 (2006).
[28] I. Ragnarsson, V. P. Janzen, D. B. Fossan, N. C. Schmeing, and R. Wadsworth, Phys. Rev. Lett. **74**, 3935 (1995).
[29] A. V. Afanasjev, D. B. Fossan, G. J. Lane, and I. Ragnarsson, Phys. Rep. **322**, 1 (1999).
[30] G. Andersson *et al*., Nucl. Phys. A **268**, 205 (1976).
[31] V. M. Strutinsky, Nucl. Phys. A **122**, 1 (1968).
[32] K. Pomorski and J. Dudek, Phys. Rev. C **67**, 044316 (2003).
[33] K. Starosta *et al*., Phys. Rev. C **64**, 014304 (2001).
[34] E. S. Paul *et al*., Phys. Rev. C **71**, 054309 (2005).
[35] I. Ragnarsson, B. G. Carlsson, Hai-Liang, A. Kardan, Purnima Singh, S. Nag, A. K. Singh, and H. Hübel, Internat. Nucl. Phys. Conf. INPC 2013, contrib. NS 185.
[36] A. O. Evans *et al*., Phys. Lett. B **636**, 25 (2006).